Cyclic Testing of Braces Laterally Restrained by Steel Studs

Oguz C. Celik[1]; Jeffrey W. Berman[2]; and Michel Bruneau[3]

Abstract: This paper experimentally investigates the cyclic inelastic performance of concentrically braced frames with and without cold formed steel stud (CFSS) infills designed to laterally restrain braces and delay their buckling. Specimens have either diagonal tube or solid bar braces with and without CFSS and U brackets providing out-of-plane and in-plane buckling restraint. Behavioral characteristics of the specimens are quantified with an emphasis on hysteretic energy dissipation. Experimental results show that, at the same ductility levels, the cumulative energy dissipation of braced frames can be significantly increased when CFSS members are used to laterally restrain the braces against buckling. However, when tubular cross sections are used for braces, local buckling led to a reduced fracture life compared to the case without CFSS members. CFSS members appear to be relatively more effective when solid bar braces having large slenderness (tension-only braces) are used, since the difference between dissipated energies obtained with and without studs is substantial.

DOI: 10.1061/(ASCE)0733-9445(2005)131:7(1114)

CE Database subject headings: Cyclic tests; Bracing; Studs; Steel frames; Seismic response; Energy dissipation; Cold-formed steel.

Introduction

Seismic behavior of concentrically braced frames (CBF), as a system, highly depends on the inelastic cyclic behavior of individual steel braces. Hysteretic loops of an axially loaded brace subject to buckling are usually unsymmetrical with degradation of the buckling strength and hysteretic energy dissipation in compression in each subsequent cycle.

Previous studies (e.g., Black et al. 1980; Ikeda and Mahin 1984; Remennikov and Walpole 1997; Lee and Bruneau 2002; Tremblay 2002) have revealed that a substantial amount of cumulative energy can be dissipated in steel braces in the postbuckling range when those members are subjected to reversed cyclic displacements. Zayas et al. (1980) experimentally demonstrated that pipe braces with lower effective slenderness (KL/r) and diameter-to-wall thickness (D/t) ratios performed better, exhibiting fuller hysteretic loops, less strength degradation, and greater resistance to local buckling. The efficiency of energy dissipation decreased rapidly after local buckling. Ikeda and Mahin (1984), based on the results of sensitivity analyses on the behavior of braced frames conducted using a physical hysteretic model, recommended the use of stocky braces over slender braces. As a result of such studies, codes require that stocky braces be used in seismically active regions. More recent research has recognized that the benefits of using braces having low slenderness ratios are somewhat offset by lower fracture life that results from the local buckling that may develop in stocky braces. Both Tremblay (2002) and Lee and Bruneau (2002) reported and quantified the degradation of compressive strength and hysteretic energy dissipation, and modified fracture life equations previously proposed by Lee and Goel (1987). In parallel, other researchers (Filiatrault and Tremblay 1998) have advocated the use of tension-only braces in seismic applications to overcome some of these problems, while recognizing that this system is possibly limited in applications for a number of reasons (Bruneau et al. 1998).

Ideally, in the perspective of seismic design, it is desirable to delay (or possibly prevent) global and local buckling of braces in steel frames. Buckling restrained braces have been developed to meet this objective of full stable and ductile hysteretic behavior without strength degradation, with low cycle fatigue. These have been implemented in the seismic design and retrofit of buildings (Clark et al. 2000; Iwata et al. 2000; Black et al. 2002; and Ko et al. 2002). This ideal is harder to achieve with conventional CBFs.

To improve the hysteretic characteristics of CBF braces, cold-formed steel studs (CFSS) of the type often used in nonstructural partition walls could be specifically designed to laterally restrain braces against buckling and enhance their seismic performance. This would require special design of CFSS members to elastically resist the out-of-plane forces developing at the onset of brace buckling.

To investigate the validity of such a solution (i.e., whether CFSS wall units could be designed to achieve the above objective, how effective they are in improving hysteretic behavior), four specimens have been designed and cyclically tested. Single square tube braces and solid rectangular solid bar X braces with and without CFSS members were tested under quasi-static cyclic displacement histories.

This paper reports on the cyclic inelastic behavior of proposed braced steel infills for steel framed buildings. The obtained strengths, stiffnesses, maximum displacement ductilities, and cumulative energy dissipation capacities are compared. Note that the infill types considered in this study could be implemented in new buildings or as a retrofitting technique in seismically vulnerable buildings lacking of strength, lateral stiffness, or ductility.

[1]Associate Professor, Division of Theory of Structures, Faculty of Architecture, Istanbul Technical Univ., Taskisla, Taksim, Istanbul 34437, Turkey; formerly, Research Scholar, Dept. of CSEE, Univ. at Buffalo, Amherst, NY 14260. E-mail: celikoguz@itu.edu.tr

[2]PhD Candidate, Dept. of CSEE, Univ. at Buffalo, Amherst, NY 14260. E-mail: jwberman@eng.buffalo.edu

[3]Director, MCEER, Professor, Dept. of CSEE, Univ. at Buffalo, Amherst, NY 14260. E-mail: bruneau@mceermail.buffalo.edu

Note. Associate Editor: Sherif El-Tawil. Discussion open until December 1, 2005. Separate discussions must be submitted for individual papers. To extend the closing date by one month, a written request must be filed with the ASCE Managing Editor. The manuscript for this paper was submitted for review and possible publication on December 30, 2003; approved on December 23, 2004. This paper is part of the ***Journal of Structural Engineering***, Vol. 131, No. 7, July 1, 2005. ©ASCE, ISSN 0733-9445/2005/7-1114–1124/$25.00.

Design of Specimens

Boundary Frames

The boundary frame dimensions were selected to be representative of bay dimensions for frames located in a test-bed structure called the "MCEER Demonstration Hospital" (Yang and Whittaker 2002). The boundary frame with an aspect ratio (L/h) of 2.0 is taken from that hospital's structural system, where L and h=bay width and height of the specimen, respectively, but actual scale of the boundary frame is 1/2 of the prototype due to limitations of the testing apparatus. However, full scale systems (with and without CFSS) would behave similarly to those tested, and deliver the same cyclic inelastic performance provided the braces have the same member slenderness, and CFSS' stiffness and strength are designed per the procedure described in a later section.

Two boundary frames previously designed and constructed by Berman and Bruneau (2003) were used but modified to accommodate different beam-to-column connections as well as steel stud and gusset connections, as described later. Additional design checks were carried out to make sure the boundary frame and its connections were safe for the contemplated applications. For one of the two boundary frames, to avoid premature low-cycle fatigue failures in the beam-to-column connections, these connections were replaced prior to testing. All the beam and column dimensions, as well as connection angles, were kept constant from specimen to specimen to allow a more uniform comparison of the strength, stiffness, and seismic energy dissipation capacity of the different proposed retrofit designs.

Infill Types

Four specimens were designed and constructed using concentric braces. Two of the specimens had closely spaced vertical cold-formed steel studs introduced to reduce the buckling length of the braces, approaching to some degree (but not perfectly) the philosophy of buckling-restrained braced frames. All specimens were designed in accordance with the AISC Seismic Provisions (AISC 2002), AISC LRFD Specifications (AISC 1999), and AISI (1996) codes as appropriate. These specimens are

- Specimen F1: CBF with single tube brace and vertical CFSS;
- Specimen F2: CBF with single tube brace and without vertical CFSS;
- Specimen F3: CBF with solid rectangular X braces and vertical CFSS; and
- Specimen F4: CBF with solid rectangular X braces and without vertical CFSS.

In Specimens F1 and F3, CFSS members were spaced at 457.2 mm (18 in.) center-to-center. All specimens were tested in the University at Buffalo's Structural Engineering and Earthquake Simulation Laboratory (SEESL).

A typical test setup for the specimens is shown in Fig. 1. The above choice of specimens made it possible to compare the seismic energy dissipation behavior of frames with either slender or stocky brace members, the latter achieved by the presence of the studs providing intermediate lateral supports both in the in-plane and out-of-plane directions and thus reducing the effective slenderness of the braces in both directions. The vertical CFSS were installed on both sides of the braces and were connected to them without bolting through the braces (to eliminate the possibility of net section fracture). The intended result was more stable, less pinched hysteretic loops with less stiffness and strength degradation under cyclic loading. In essence, the objective was to use common nonstructural elements (such as steel stud walls), slightly modified, to help enhance the seismic behavior of a common CBF to near that of an idealized buckling prevented (or axially yielding) brace with hysteretic behavior.

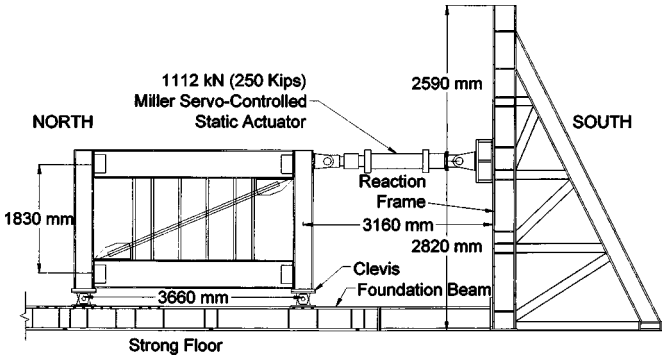

Fig. 1. Typical test setup for specimens

Since the fracture life of tube braces may be reduced significantly due to local buckling effects, one could question the usefulness of preventing global buckling of tubular braces. Specimens F1 and F2 allow a comparison of the fracture life of tube brace systems having low and high effective slenderness ratios.

Materials

ASTM A572 Gr.50 steel was used for the boundary frame. Locally available, 12 gauge, 228 MPa (33 ksi) yield point CFSS products were used in this research. Properties for the light gauge studs used here were taken from the Dietrich Product Data (2001). The solid bar braces, gussets, and angle connectors for the studs were also ASTM A572 Gr.50. U brackets used as in-plane buckling restrainers were ASTM A36 grade steel. The tube material was ASTM A500 Gr.B with minimum yield stress of 317 MPa (46 ksi). Bolts used are A490 grade in gussets-to-boundary-frame connections, and A307 grade for all other connections of the infills.

ASTM Standard coupon tests (ASTM 2002) gave average values of yield stresses of 377 MPa for solid braces and 385 MPa for the tubes. The yield strength of the tube brace coupons was calculated using a 0.2% strain offset, since this steel exhibited no definite yield plateau. The solid bar coupons had an elastic-plastic behavior. These material data were used in static pushover analyses of the specimens conducted using *SAP2000* (CSI 1998) to predict the load-displacement curves of the specimens.

Details of Specimens

Double web-angle beam-to-column connections were welded to the beam web using typical 8 mm fillet welds all around the angle legs. The upper and lower welds on the beams were terminated at 25 mm from the face of the other leg. Connection to the column flanges used six 31.75 mm $\left(1\frac{1}{4}\text{ in.}\right)$ diameter A490 bolts. Column bases were connected to clevises via endplates which were welded to the columns and bolted to the clevises. Further details regarding the specimens can be found in Celik et al. (2004).

Braces were designed to be the largest possible that could be tested without exceeding the maximum force capacity of

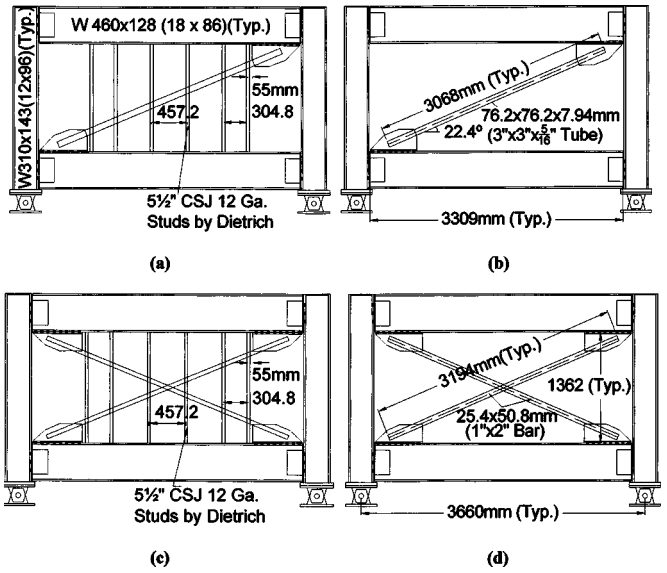

Fig. 2. Schematic of specimens: (a) F1; (b) F2; (c) F3; and (d) F4

1,112 kN (250 Kips) of the largest actuator available in the laboratory, with a safety factor of 1.50, and taking strain hardening effects into account. As a result, a single tube brace of 76.2 mm by 76.2 mm (3 in.×3 in.) with t=7.94 mm (5/16 in.) wall thickness, and solid X braces having a cross section of 25.4 mm by 50.8 mm (1 in.×2 in.), were selected. Tube braces had 431.8 mm long and 12.7 mm wide slots at each end for welded connections to the gussets. Specimens F1–F4 are illustrated in Figs. 2(a–d), respectively.

Cold-formed steel studs used in Specimen F1 and Specimen F3 were $5\frac{1}{2}$ in. CSJ 12 gauge by Dietrich (2001). Cold-formed stud-to-beam connection details for Specimens F1 and F3 are shown in Figs. 3(a and b). Nuts for the bolts used in stud-to-angle, angle-to-beam, and stud-to-stud connections were in the snug-tight condition.

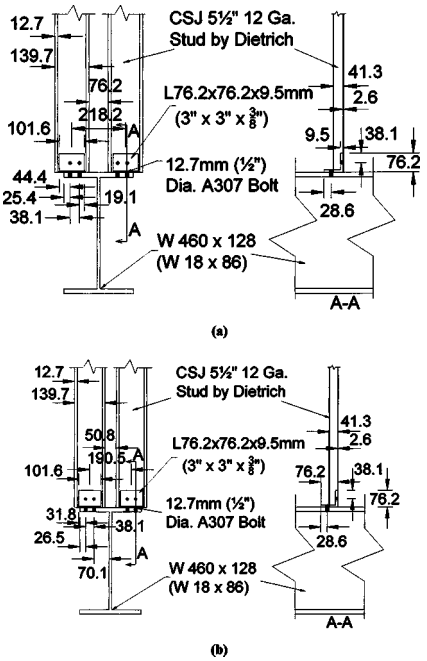

Fig. 3. Cold-formed steel stud-to-beam connection details: (a) F1; and (b) F3

The design of the vertical CFSS had two requirements, namely stiffness and strength. The minimum stiffness and design load for the CFSS was determined using the procedure originally given in Winter (1960), revisited in Yura (1993, 1994), and summarized in Salmon and Johnson (1996). Required stiffnesses and design loads for the CFSS members were obtained as follows.

- Determine the ideal CFSS stiffness, k_{ideal}, from (Yura 1993)

$$k_{\text{ideal}} = \frac{\beta P}{L} \tag{1}$$

  where β=parameter which varies nonlinearly with the number of spans the lateral bracing creates (β=1 for one span, β=4 for four or more spans as is the case here), P=brace compression capacity calculated using the unbraced length provided by the studs, and L=unbraced length of the brace. The minimum required stiffness, k_{req}, is then conservatively taken as twice k_{ideal}.
- Determine the minimum cross-sectional area and moment of inertia for the studs from the previously determined minimum required stiffness. Note that the studs have been configured to provide in-plane lateral bracing, which creates axial load in the studs and requires a minimum cross-sectional area, and out-of-plane lateral bracing, which imparts shear and moment on the studs and requires a minimum moment of inertia.
- Determine the design force, Q_n, to be applied to the studs where they intersect the braces as

$$Q_n = k_{\text{ideal}}(0.004L) \geq 0.05P \tag{2}$$

  which assumes that the out-of-plumbness of the braces and the accidental eccentricities amount to initial brace imperfections of $L/250$. Q_n is applied to the studs in both the vertical and out-of-plane horizontal directions.

After selecting a CFSS that met the stiffness requirements and determining the design loads, the limit states given in AISI (1996) were used to determine the CFSS strength. Lateral torsional buckling, flexural torsional buckling, and web crippling are all considered in that standard. The connections of the studs to the boundary frame and braces were designed for the loads resulting from the simultaneous application of Q_n in the vertical and out-of-plane horizontal direction. Connection capacities were determined using AISI (1996) and AISC (1999), although it should be mentioned that local flange bending of the studs at the connection to the braces was not considered.

Details regarding custom made U brackets used as in-plane buckling restrainers are given in Figs. 4(a and b). Essentially two

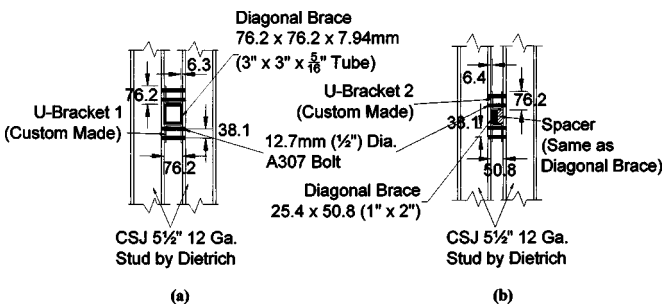

Fig. 4. U-brackets-to-cold formed steel stud bolted connection details: (a) F1; and (b) F3

types of U brackets were designed for each specimen with CFSS. The distinctive feature of the connection detail around the brace and CFSS intersection region is that there is no mechanical connection to the braces. CFSS members are connected to each other via their inner flanges using a long, 12.7 mm diameter bolt passing through the holes in the brackets. U brackets and CFSS members were to be in perfect contact with the brace surfaces to provide a direct load transfer. Small spacers having the same section of the bar brace were used in Specimen F3 to fill the gap in the connection.

Cyclic Testing of Specimens

Each specimen was subjected to quasi-static cyclic loading in accordance with the ATC-24 (1992) protocol. Since the top horizontal displacement of the specimens is directly related to the brace axial displacement, this horizontal value was taken as the displacement control parameter for all tests. As the study of cyclic inelastic buckling behavior of the brace elements was the objective of this study, special care was taken during the tests to identify the point of buckling initiation for the braces. In Specimen F1, in which the tension yield and buckling strengths of the brace were close to each other, the load was first applied to have tension in the brace, and in the above procedure, the experimentally obtained δ_y (specimen top horizontal displacement at the onset of brace tension yielding) was taken as the test control parameter. To facilitate comparison between the results obtained for Specimens F1 and F2 in subsequent sections, the same cyclic displacement history that was applied to Specimen F1 (i.e., absolute displacement values) was applied to Specimen F2. On the contrary, in Specimen F3 in which tension yield and buckling strengths of the restrained X braces were significantly different from each other, with buckling occurring first, in the above procedure, the experimentally obtained δ_b (specimen top horizontal displacement at the onset of brace buckling) was taken as the test control parameter. Again, to facilitate comparisons between Specimens F3 and F4, the same cyclic displacement history that was applied to Specimen F3 was applied to Specimen F4.

Yield and buckling values of specimen's forces and displacements were analytically estimated by static pushover analysis using *SAP2000*, and were used to initially control the tests. However, the experimentally obtained values were used as test control parameters beyond the elastic range. These were determined at the onset of visible nonlinearity in the force-displacement curve, or by the point from which the actuator force tended to drop abruptly (during buckling). The magnitude of the cyclic displacement histories of the specimens are presented in Table 1.

Table 1. Cyclic Displacement Histories of Specimens

Displacement step	Number of cycles	Cumulative number of cycles	Displacement Δ/δ_y	Displacement (mm)	Drift (%)
(a) Specimen F1					
1	3	3	0.33	3.8	0.16
2	3	6	0.67	7.6	0.32
3	3	9	1	11.4	0.48
4	3	12	2	22.8	0.96
5	3	15	3	34.2	1.44
6	2.5	17.5	4	45.6	1.92
(b) Specimen F2					
1	3	3	0.33	3.8	0.16
2	3	6	0.67	7.6	0.32
3	3	9	1	11.4	0.48
4	3	12	2	22.8	0.96
5	3	15	3	34.2	1.44
6	2	17	4	45.6	1.92
7	4	21	5	57.0	2.40
8	0.5	21.5	6	68.4	2.88
(c) Specimens F3 and F4					
1	3	3	0.20	2.4	0.11
2	3	6	0.43	5.1	0.23
3	3	9	0.76	9.1	0.41
4	3	12	1	11.9	0.54
5	3	15	2	23.8	1.08
6	3	18	3	35.7	1.62
7	2	20	4	47.6	2.16

Experimental Observations

The behavior of each specimen, both in the elastic and inelastic ranges, is discussed below and summarized in Table 2. Cyclic tests were also performed on the bare frames to characterize their hysteretic behavior. The bounding surface model developed by Dafalias and Popov (1976) was used to model the bare frame cyclic behavior. To fit the experimental data, modeling parameters needed to develop the hystereses were calculated. Numerical results showed that the error in the dissipated cumulative energy was less than 10% between the modeled and tested boundary frames. In all cases, experimental base shear force versus drift hysteresis curves are shown in Fig. 5, and results for the case of infill only (i.e., after subtracting the contribution of the bare frame) are illustrated in Fig. 6. All details on the procedure used to model and subtract the bare frame contribution can be found in Berman and Bruneau (2003) and Celik et al. (2004).

Specimen F1

Specimen F1 was first subjected to a lateral load producing tension in the brace (note that the same convention was adopted for Specimen F2). Up to 0.96% drift ($2\delta_y$), the specimen did not show significant deterioration in strength and stiffness, in other words, the behavior was almost cyclic symmetric with comparable axial yielding in tension and compression.

Beyond this drift level, the shape of the hysteresis curves for Specimen F1 gradually became one-sided upon repeated inelastic buckling of the tubular brace member. However, the difference between the buckling and tension strengths in each cycle was still significantly less than would be expected in the absence of lateral bracing by the studs.

At 1.44% drift ($3\delta_y$), a decrease in buckling strength was observed due to the development of local buckling in the tube. On the tension side, as expected from the coupon tests, strength increased at each displacement cycle until fracture started to develop. The ratio of the maximum achieved base shear (brace in tension) to the yield base shear is 1.32. Deterioration of the brace postbuckling resistance at various drift levels was relatively slow. During the first excursions of compression cycles at 0.96, 1.44, and 1.92% drifts, the ratio of the compression strength at that cycle to the peak compression strength reached during the test

Table 2. Behavioral Characteristics of Tested Specimens

Specimen	Total initial stiffness (kN/mm)	Initial stiffness-infill (kN/mm)	Yield or buckling base shear (kN)	Yield or buckling displacement (mm)	Maximum drift (%)	μ	$K_{exp}/K_{theoretical}$	Total energy (kN m)	Infill energy (kN m)
F1	88.8	78.2	636.1	11.4	1.92	4	1.08	274	227
F2	61.4	51.0	511.5	10.2	2.88	6[a]	1.81[c]	310	192
F3	136.0	125.7	898.5	11.9	2.16	4	0.97	205	169
F4	106.6	96.3	182.4	3.0	2.16	4[b]	1.25	95	37

[a]Reached displacement ductility based on the yield displacement of Specimen F1.

[b]Reached displacement ductility based on the buckling displacement of Specimen F3.

[c]This difference comes from the increase in the brace clear length due to inelastic gusset behavior.

dropped to 1.00, 0.93, and 0.74. Ratios at the same drift levels for the infill only case are 1.00, 0.87, and 0.60. Strain gauge data showed that 2% strain was reached in the brace at 1.92% drift. A displacement ductility ratio (μ) of 4 was achieved when the tension and compression strengths of the specimen were, respectively, 100 and 67% of the maximum values obtained experimentally. As seen from Table 2, the contribution of the infill to the initial stiffness is 88%. After several cycles at displacement levels greater than the yield displacement, bearing failure of the intermediate studs led to loss of contact between the buckling restrainers and the brace, which resulted in reduced base shear strength and system stiffness.

Furthermore, the elastic experimental effective length factor (K) was calculated to be 1.08, compared to a theoretical value of 1.00 (taking L as the diagonal distance between stud centers). This value has been obtained using the measured tube strain gauge data, at axial strains below the yield level, to calculate the bending moment diagram on the brace; the maximum of the distances between two successive inflection points on the deflected shape (points of zero moment on the bending moment diagram) was taken as the effective length of the brace.

Fig. 5(a) also shows the theoretical pushover envelope curves obtained using the axial plastic hinge properties proposed by FEMA 368 (2001) (including the bare frame contribution) super-

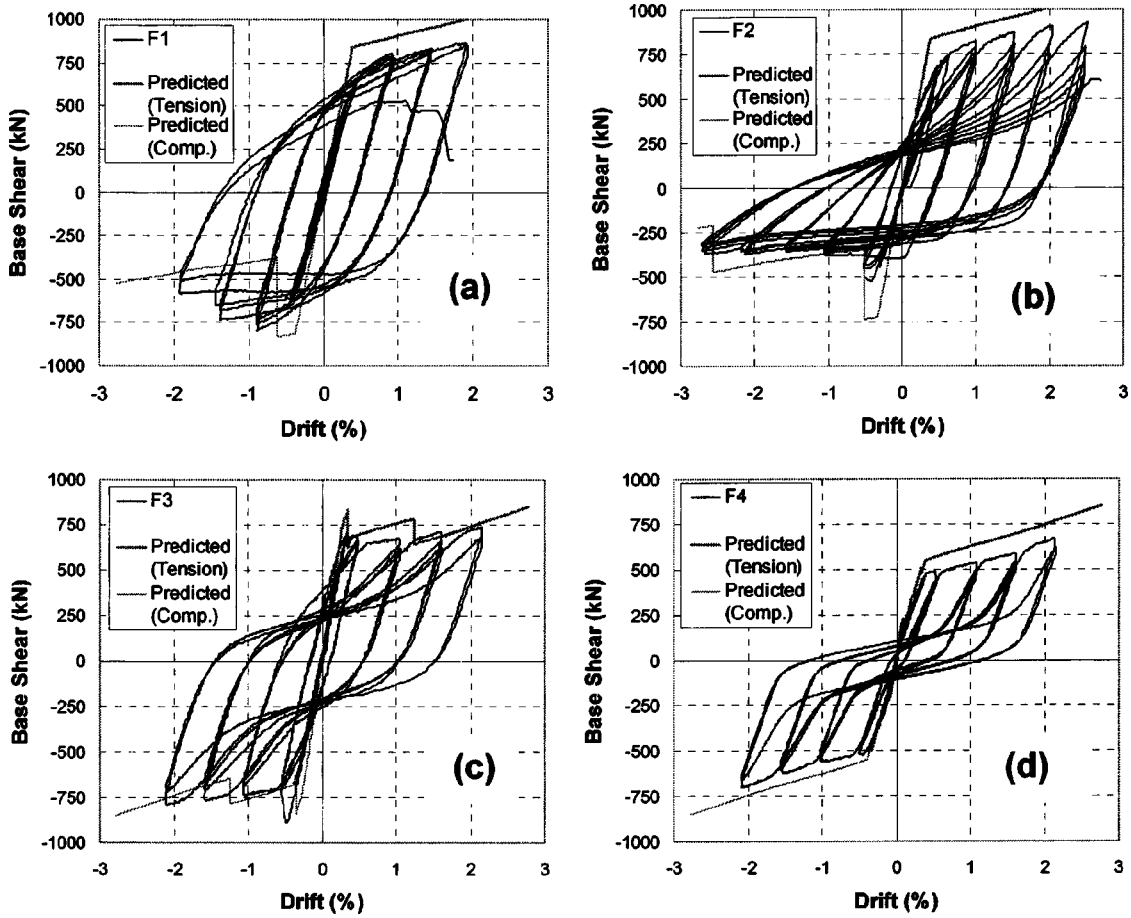

Fig. 5. Experimental hysteresis and predicted pushover curves for specimens: (a) F1; (b) F2; (c) F3; and (d) F4

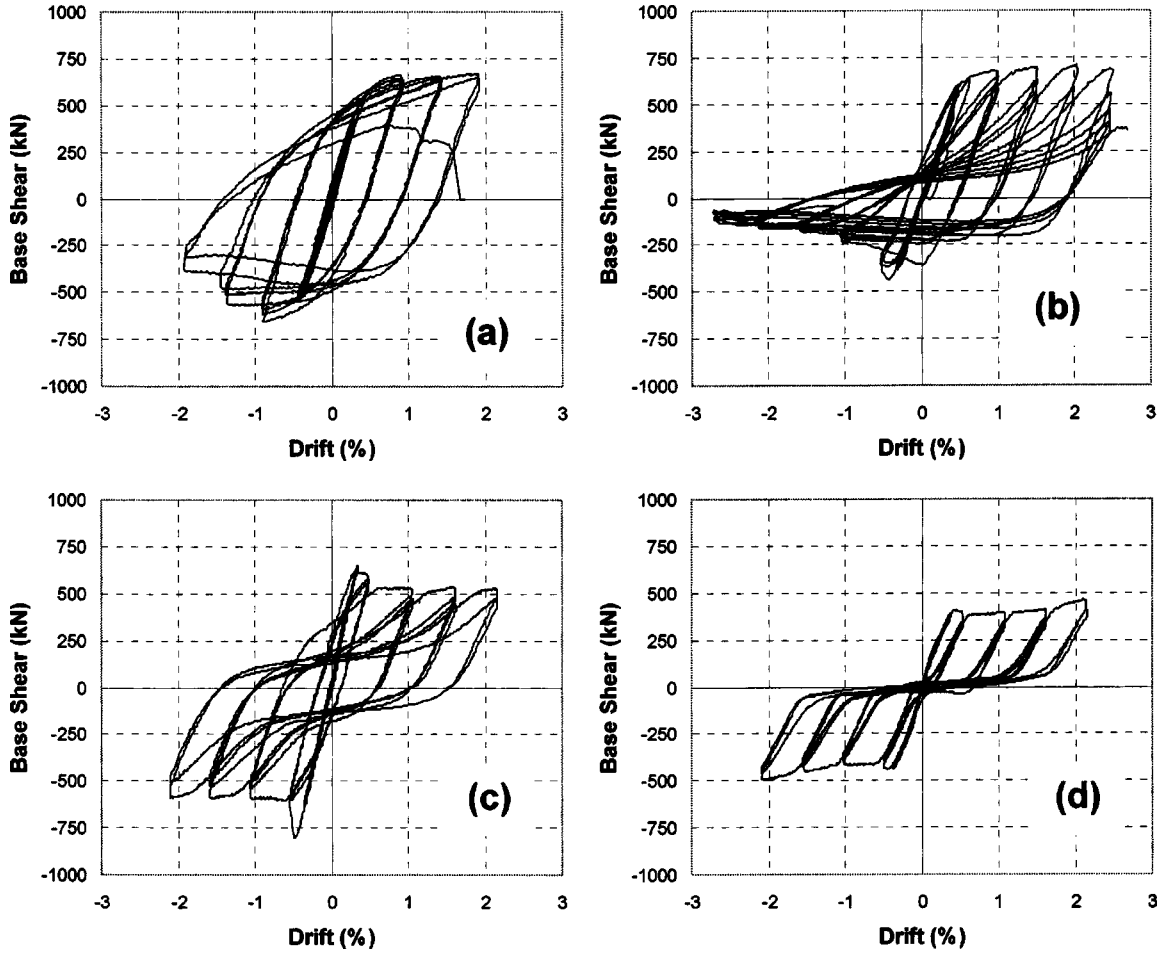

Fig. 6. Comparison of base shear versus drift hysteresis curves for infills: (a) F1 ($KL/r=19.7$); (b) F2 ($KL/r=77.3$); (c) F3 ($KL/r=65.5$); and (d) F4 ($KL/r=195.7$)

imposed on top of the hysteretic curves. The initial stiffness and the base shear at brace buckling are, respectively, approximately 35 and 5% overpredicted by FEMA 368. On the tension side, the maximum achieved base shear is about 16% overpredicted. These differences may be attributed to FEMA 368 modeling assumptions. Fuller hysteretic loops indicate that the contribution of the brace in compression to the total energy dissipation is substantial, and greater than predicted by FEMA 368.

The out-of-plane buckling mode of the brace (Cycle 15, $-3\delta_y$), a general view (Cycle 16, $-4\delta_y$), development of local buckling in middle brace segment (Cycle 16, $-4\delta_y$), and fracture of tube brace middle section (Cycle 18, $+4\delta_y$) are shown in Fig. 7.

Specimen F2

Specimen F2 was subjected to the same displacement history as Specimen F1 to facilitate comparison of the relative hysteretic energy dissipation capacity of the two specimens. However, additional cycles were performed for Specimen F2 beyond the maximum displacements reached for Specimen F1, until failure, to allow determination of the fracture life of the tube brace. Specimen F2 exhibited ductile and stable cyclic behavior up to 2.40% drift, although some pinching is obvious in the hystereses. Up to 0.48% drift, the hystreresis curves are cyclic symmetric, however, in the aftermath of brace buckling, they become one-sided due to the deterioration in buckling strength. On the tension side, strength increases until fracture develops. The ratio of the maximum tension strength to the yield strength is 1.26.

During the first excursions of compression cycles at 0.48, 0.96, 1.44, 1.92, and 2.40% drifts, the ratio of the compression strength at that cycle to the peak compression strength reached during the test dropped to 1.00, 0.76, 0.58, 0.46, and 0.44. For the infill-only case, ratios at the same drifts were 1.00, 0.82, 0.53, 0.47, and 0.46. Note that the largest relative deterioration in buckling strength occurred at the two drift steps just after the first buckling cycles. During the following cycles, there was no significant change in this ratio since it began to stabilize. Residual buckling strengths of 0.59 (total frame) and 0.16 (infill) were obtained at the last compression cycles prior to fracture versus a proposed constant value of 0.40 given in FEMA 368 (2001). Strain gauge data showed that 1.5% strain was reached in the tubular brace at 2.50% drift. Specimen F2 exhibited a displacement ductility ratio (μ) of 6 when the tension and compression strengths were 65 and 46% of the maximum achieved peak strengths.

Table 2 shows that the contribution of the brace to the initial stiffness is 83%. The experimental elastic K factor obtained following the same procedure as for Specimen F1 was found to be 0.90 compared to a theoretical value of 0.5 (taking L as the clear brace length between gussets).

The initial stiffness and the base shear at brace buckling shown in Fig. 5(b) are approximately 93 and 41% overpredicted, respec-

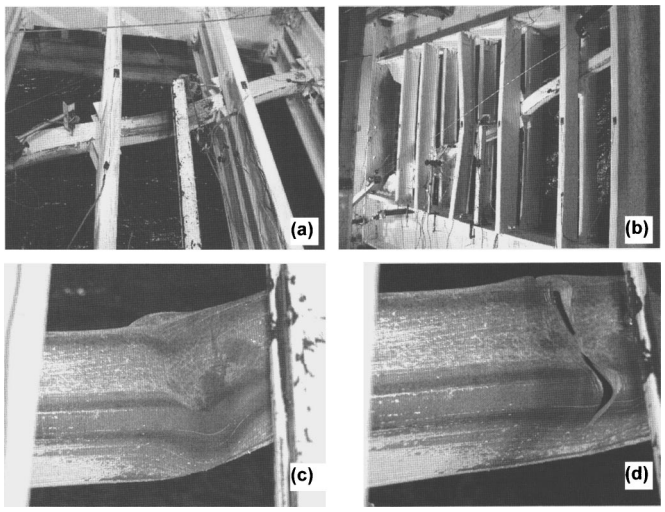

Fig. 7. Damage level in Specimen F1: (a) out-of-plane buckling mode of brace (Cycle 15, $-3\delta_y$); (b) general view (Cycle 16, $-4\delta_y$); (c) development of local buckling in middle brace segment (Cycle 16, $-4\delta_y$); and (d) Fracture of tube brace middle section (Cycle 18, $+4\delta_y$)

tively, by the theoretical pushover curves. On the tension side, the maximum achieved base shear is about 11% overpredicted.

A general view of the buckled brace (Cycle 16, $-4\delta_y$) and local buckling at midbrace length (Cycle 19, $-5\delta_y$) is shown in Fig. 8.

Fracture Life of Specimens F1 and F2

Experimental fracture life ($\Delta_{f,\text{exp}}$) of tube braces can be obtained from hysteretic curves following the procedure proposed by Lee and Goel (1987). The steps of this procedure are

- Hysteresis curves are normalized by yield strength and the corresponding yield displacement;
- The tension branch of the hysteresis is divided into two regions, Δ_1 and Δ_2, defined at 1/3 of the yield strength. Δ_1 = tension deformation from the load reversal point to 1/3 of the yield strength point displacement, while Δ_2 is from 1/3 yield strength point to the unloading point; and
- Experimental fracture life is then calculated using

$$\Delta_{f,\text{exp}} = \sum (0.1\Delta_1 + \Delta_2) \tag{3}$$

Experimental values of $\Delta_{f,\text{exp}} = 32.9$ and 64.7 were found for Specimens F1 and F2, respectively. Note that the cycles at $3\delta_y$ (1.44% drift) and above most contributed to the fracture life (83% of the total in Specimen F2).

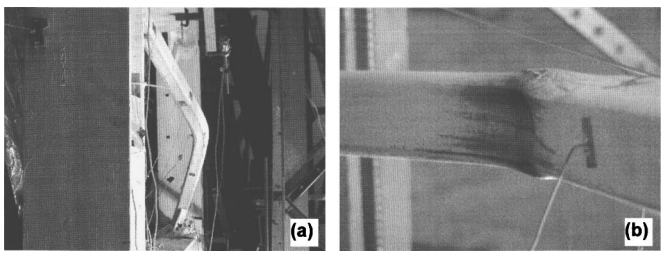

Fig. 8. Damage level in Specimen F2: (a) general view (Cycle 16, $-4\delta_y$); and (b) local buckling at mid-length (Cycle 19, $-5\delta_y$)

Theoretical fracture lives (Δ_f) introduced in Lee and Goel (1987) and Archambault et al. (1995) methods were also calculated. The Lee and Goel model is given by

$$\Delta_f = C_s \frac{(46/F_y)^{1.2}}{[(b-2t)/t]^{1.6}} \left(\frac{4b/d+1}{5} \right) \tag{4}$$

where $C_s = 1{,}560$ (a numerical constant), F_y = yield stress (ksi), b = gross width of section, d = gross depth of section, and t = thickness of section, and the Archambault et al. model is given by

$$\Delta_f = C_s \frac{(317/F_y)^{1.2}}{[(b-2t)/t]^{0.5}} \left(\frac{4b/d+1}{5} \right)^{0.8} \times (70)^2$$

$$\text{for } KL/r < 70 \tag{5a}$$

$$\Delta_f = C_s \frac{(317/F_y)^{1.2}}{[(b-2t)/t]^{0.5}} \left(\frac{4b/d+1}{5} \right)^{0.8} \times (KL/r)^2$$

$$\text{for } KL/r \geq 70 \tag{5b}$$

where $C_s = 0.0257$, where all other parameters are as defined above but F_y is in MPa.

Numerical values of $\Delta_f = 48.2$ and 36.1 were obtained for the Lee and Goel and the Archambault et al. methods, respectively, for Specimen F1, and 48.2 and 43.9 for Specimen F2, using the experimentally obtained values of K. The ratios of the experimental to theoretical values for these two models are 0.68 and 0.91 for Specimen F1, and 1.34 and 1.47 for Specimen F2. For Specimen F1, the Archambault et al. method agrees reasonably well with the experimental one. For Specimen F2, both methods underestimate the fracture life of the tube brace, and the Lee and Goel model gives closer results in this case.

Specimen F3

Specimen F3 was first loaded towards the south, producing tension in the west-side brace and compression in the east-side brace. Up to approximately 0.50% drift, the specimen did not show deterioration in strength and stiffness. At the onset of buckling of the east side brace segment between the fourth and the fifth studs (counting from the north), the base shear dropped abruptly. The peak base shear force during test was reached prior to this buckling. After buckling, the hysteresis for Specimen F3 stabilized and fuller curves on both tension and compression sides developed. Negative and positive base shear forces reached were the same for practical purposes, which is attributable to the symmetric X brace configuration of the specimen. For negative and positive base shears, absolute ratios of the maximum negative and positive base shears at final cycles to the peak base shear at brace buckling are 0.89 and 0.83, respectively. Base shear forces gradually increased during the first cycle of each displacement increment and decreased slightly during the second and third cycles thereafter.

The overall behavior of Specimen F3 was ductile and stable up to 2.16% drift, although pinching in the hysteretic loops is apparent. During the second and third cycles at each imposed drift level, the hysteresis curves tended to meet at the peak point (peak oriented hysteretic curve) of the previously obtained hysteresis.

Variation in the negative base shear (in the direction of the initially buckled brace in compression) illustrates the deterioration of brace postbuckling resistance at various drift levels. However, since one of the braces was always in tension and the bare frame strain hardened, the total base shear actually increased at

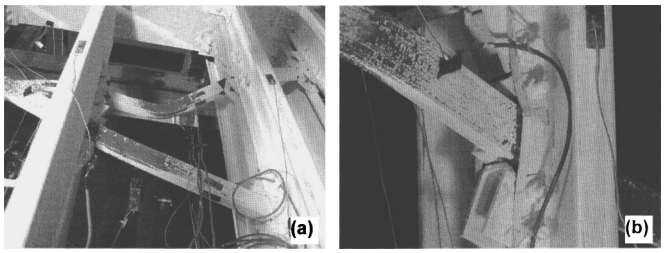

Fig. 9. Damage level in Specimen F3: (a) yielding in tension and compression braces (Cycle 17, $3\delta_y$); and (b) yielding of braces and bearing failure in studs (Cycle 20, $-4\delta_y$)

large displacements. In fact, during the first excursions of compression cycles, the ratio of the negative base shear (total specimen) at that cycle to the negative peak base shear at 0.54, 1.08, 1.62, and 2.16% drifts dropped to 1.00, 0.83, 0.85, and 0.89. For the infill-only case, the same ratios were 1.00, 0.75, 0.73, and 0.73.

Similarly, for the positive base shear side, the same ratio (with the positive peak shear) at the same drifts reached 1.00, 0.94, 0.99, and 1.03, and for the infill-only case were 1.00, 0.82, 0.82, and 0.81. Strain gauge data showed that the bar braces exhibited stable energy dissipation up to 2.16% drift, producing about 3% maximum strain (including axial and bending effects) in the midlength of the east side brace. In other parts of the braces, maximum 1.5% axial strains were reached (average axial strain was 1.02%), which indicates that the bar braces underwent significant plastic deformations. A displacement ductility ratio (μ) of 4 was achieved without any significant strength and stiffness degradation with the exception of initial buckling values. After several cycles at displacement levels greater than the buckling displacement, bearing failure of the intermediate studs led to loss of contact between the buckling restrainers and the brace, resulting in reduced base shear strength and system stiffness.

Table 2 indicates the substantial increase in stiffness for this specimen. The contribution of the infill to the initial stiffness is 92%. Furthermore, an experimental elastic effective length factor (K) of 0.97 was obtained for a length L taken as the diagonal distance between the stud centers. The strain gauge data for Specimen F3 were used to calculate this elastic experimental K factor.

Fig. 5(c) also demonstrates the predicted pushover curves obtained using FEMA 368 superimposed on the hysteretic curves of Specimen F3. The initial stiffness and the negative base shear at brace buckling are approximately 11% overestimated and 6% underestimated, respectively. Pushover analysis curves match reasonably with the experimental results. This could be attributed to the fact that the material properties of solid bar brace members are more bilinear and therefore better modeled by the selected bilinear material model (with strain hardening), which was incorporated into the analysis.

Yielding in tension and compression of braces (Cycle 17, $3\delta_y$) and yielding of braces and bearing failure in Studs (Cycle 20, $-4\delta_y$) are depicted in Fig. 9.

Specimen F4

Specimen F4 was subjected to the same displacement history as Specimen F3 to allow comparison of the respective hysteretic energy dissipation. The hysteresis for Specimen F4 is fairly symmetrical in the elastic and inelastic cycles. The overall behavior of Specimen F4 was ductile and stable up to 2.16% drift, although significant pinching is visible in the hystereses.

These slender braces behaved like tension-only braces during testing due to their negligible buckling strength. Therefore, although they resisted some degree of compression force up to the onset of buckling, this strength did not contribute significantly to the overall shape of the hysteresis curves. During subsequent cycles, an increase in the base shear strength was apparent from the hyteresis, as illustrated in Fig. 5(d). This is actually due to the boundary frame contribution as evidenced by comparing Figs. 5(d) and 6(d). In fact, the infill hysteresis exhibits near elastic-plastic behavior (during each excursion) up to the application of the last cycle (2.16% drift). The ratio of the maximum tension strength to the strength at the displacement level of Specimen F3 buckling is 1.28.

During the first excursions of each imposed drift level, the ratio of the maximum positive and negative base shear during that cycle to the strength at buckling at 0.54, 1.08, 1.62, and 2.16% drifts reached 1.00, 1.10, 1.20, and 1.36. For the infill-only case, these ratios were 1.00, 0.98, 1.01, and 1.14. For the negative side of the hystereses, the corresponding ratios were 1.00, 1.07, 1.20, and 1.34 for the total frame, and were 1.00, 0.94, 1.03, and 1.12 for the infill only case. Up to 1.7% strain was reached in the bar braces at 2.16% drift. Hysteretic loops show that energy was dissipated by tension yielding rather than brace buckling. Specimen F4 exhibited a displacement ductility ratio (μ) of 4.

Table 2 (presented earlier) shows that the contribution of the bar braces to initial stiffness is about 90%. An experimental elastic K factor of 0.63 was found for a L value taken as the clear brace length between the gussets.

The initial stiffness and the negative base shear at brace buckling from the theoretical pushover curves using FEMA 368 axial plastic hinges are approximately 29 and 7% overestimated, respectively. Although theoretical results on the negative base shear side match reasonably with the experimental results, relatively larger differences were obtained on the positive side. Again, this could be attributed to the modeling issues in FEMA 368, and, partly, behavioral differences of the boundary frame under cyclic loading.

A general view of damage in the specimen (Cycle 18, $-3\delta_y$) is shown in Fig. 10.

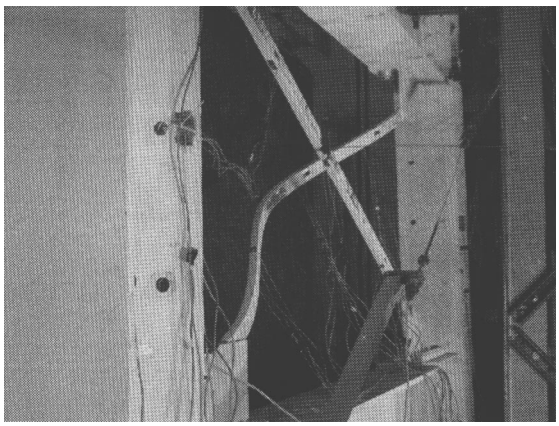

Fig. 10. Damage level in Specimen F4 (Cycle 19, $4\delta_y$)

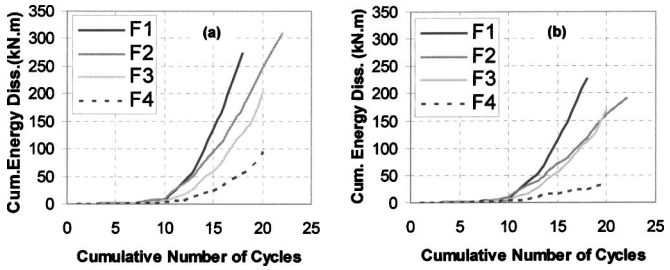

Fig. 11. Comparison of cumulative energy dissipation for specimens: (a) for total frame; and (b) for infill only

Hysteretic Energy Dissipation

For any cycle, the area under the experimentally obtained hysteretic curve gives the dissipated energy through inelastic behavior. Since the cumulative energy dissipation is a useful measure of the seismic efficiency of a structural system, these values were calculated, and the variation of cumulative energy dissipation with cumulative number of cycles are plotted in Fig. 11 for the total frame and infill-only cases. Fig. 11 and Table 2 show that, for Specimen F1, 83% of the total energy was dissipated by the infill versus 17% for the boundary frame. In Specimen F2, 62% of the total energy was dissipated by the infill versus 38% for the boundary frame. For Specimen F3, 82% of the total energy was dissipated by the infill versus 18% for the boundary frame. For Specimen F4, these numbers are 39 and 61%, respectively. Inelastic behavior of the beam-to-column double angle connections was observed at large drift ratios, which explain the appreciable contribution of the bare frame to the cumulative energy dissipation at larger drifts seen in Fig. 11.

Summary and Comparison

Using experimental hystereses, some behavioral characteristics of Specimens F1, F2, F3, and F4 are summarized and compared in this section. Total initial stiffness, initial stiffness of infill, yield or buckling base shear, yield or buckling displacement, maximum attained percent drift, achieved displacement ductility, and cumulative energy dissipations by component (total and infill-only) are quantified in Table 2 presented earlier. To better compare the effectiveness of each specimen, normalized values of base shear and energy dissipation (infill-only) were calculated and given in Table 3. Cumulative hysteretic energy dissipation was normalized as follows:

$$E_{HN} = \frac{E_H}{V_y \delta_y} \tag{6}$$

where E_{HN} = normalized cumulative hysteretic energy dissipation, E_H = cumulative hysteretic energy dissipation, V_y = yield (or buckling) base shear, and δ_y = experimentally obtained yield or buckling displacement. Note that, for the purpose of normalization, the average peak base shears reached in the positive loading direction at each of the large plastic deformation cycles was used for the value of V_y, and the experimental yield displacement was used for Specimens F1 and F2. For Specimens F3 and F4, because the maximum base shear strength drops after first buckling, the average of the base shears reached in the subsequent cycles only was used to define V_y, and the experimental buckling displacement was used for δ_y (i.e., δ_b).

Table 3. Normalized Characteristics of Tested Specimens (Infill-Only)

Specimen	V_y (kN)	δ_y (mm)	$E_{H,\text{infill}}$ (kN mm)	$V_y/(V_{y,\text{F1}})$	E_{HN}
F1	661.3	11.4	227,000	1.00	30.1
F2	673.0	11.4	192,000	1.02	25.0
F3	592.3	11.9	169,000	0.90	24.0
F4	442.0	11.9	37,000	0.67	7.0

Table 3 shows that braces having CFSS members had greater hysteretic energy dissipation. Cumulative hysteretic energy was the greatest in Specimen F1, although this specimen had less maximum displacement ductility due to its lower fracture life as compared to Specimen F2.

Hysteretic behavior of all specimens is shown in Fig. 6. Variation of cumulative energy dissipation with cumulative number of cycles for all specimens, after subtraction of the boundary frame contributions, is shown in Figs. 11(a and b) for comparison purposes.

Specimen F1 achieved the maximum hysteretic energy dissipation for the infill alone. Percent energy dissipation amounts for other specimens are 85, 74, and 16% of Specimen F1 for Specimens F2, F3, and F4, respectively.

Specimen F2 dissipated the largest amount of total hysteretic energy, essentially due to its higher fracture life. A displacement ductility of 6 was reached prior to fracture, the largest value for all specimens tested (but Specimens F3 and F4 were not tested up to failure to save the boundary frames). Infill (tube brace) failure occurred at the brace to gusset connection in the net section area. The out-of-plane buckling displacements of the brace were significant, in excess of 10% of the brace clear length. Although residual out-of-plane displacements caused significant strength degradation in compression, the behavior was ductile and stable.

Solid bar braces in Specimen F3 dissipated a relatively moderate amount of energy with ductile but pinched hysteretic curves. Up to a displacement ductility of 4, the braces dissipated energy by yielding and buckling under reversed displacement cycles. CFSS members and U brackets reduced the buckling length of the braces effectively. After initial buckling of the east side brace when the peak base shear was obtained, strength degradation stabilized under subsequent cycles.

The least amount of cumulative energy was dissipated by Specimen F4. The hysteresis curves were stable yet significantly pinched, as expected. Energy was essentially dissipated through the yielding of the braces in tension only. A displacement ductility of 4 was reached without any visible damage. Note that the largest out-of-plane displacements were obtained for this specimen, in excess of 14% of the brace clear length.

The maximum drift reached by Specimen F2 was 2.88%. Specimens F1, F3, and F4 exhibited maximum drifts of 1.92, 2.16, and 2.16%, respectively.

Although the above comparisons refer to absolute cumulative hysteretic energies, the trends remain the same for normalized cumulative hysteretic energies, since, as shown in Table 3, normalized energies for Specimens F3 and F4 are less than those for Specimens F1 and F2. This is illustrated in Fig. 12(a).

Hysteretic energy dissipation per brace volume used can be another measure to compare the relative effectiveness of these specimens. Shown in Fig. 12(b) is the variation of volumetric energy dissipation versus cumulative number of cycles. Peak energy per volume values of 0.049, 0.041, 0.028, and 0.006 kN mm/mm^3 are found for Specimens F1, F2, F3, and F4, respectively (although the last two specimens were not tested to

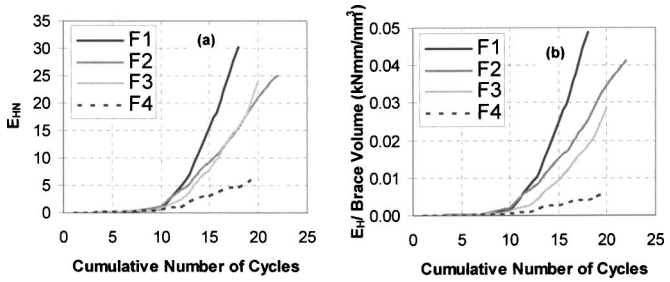

Fig. 12. Comparison of energy dissipation (infill-only): (a) normalized cumulative energy dissipation; and (b) cumulative energy dissipation per brace volume used

failure). Additionally, at a common ductility of 4, these values become 0.049, 0.025, 0.028, and 0.006 kN mm/mm^3, which show that braces having CFSS had better hysteretic energy dissipation capacity.

Conclusions

The major conclusions reached from this experimental study of CBF with and without vertical CFSS members are as follows:

1. Specimen F1 (concentrically braced frame with single tube brace and vertical CFSS members) achieved superior behavior over the other specimens in terms of infill cumulative hysteretic energy dissipation at given drift values. Maximum displacement ductilities (μ) attained for Specimens F1 and F2 are 4 and 6, respectively. Experimental fracture life of the tube in Specimen F2 was higher than that of the tube in Specimen F1, as reducing the buckling length for tubular cross-section braces also accelerated their local buckling.
2. The use of CFSS and U brackets as buckling restrainers was more effective in tension-only braced frames than in tension-compression braced frames. The relative increase in energy dissipation for the tension only systems (i.e., the increase in energy dissipated in Specimen F3 versus Specimen F4) was significantly larger than the relative increase for tension compression systems (i.e., the increase when considering Specimen F1 versus Specimen F2). Moreover, provided that all brace connections are able to elastically resist forces corresponding to brace yielding, solid braces and/or tension only systems may be able to sustain larger amounts of reversed axial cyclic displacements, since local buckling is not likely to occur.
3. Using dissipated hysteretic energy per brace volume to compare the relative effectiveness of these specimens showed that braces having CFSS had better hysteretic energy dissipation capacity.
4. Structural use of CFSS members as out-of-plane buckling restrainers also helped reduce the out-of-plane displacements of braces. This would minimize the wall cladding damages that may occur as a result of large lateral displacements during buckling of braces under severe earthquake excitations. Performance of CFSS members in Specimen F3 was better than the ones in Specimen F1, which could be attributed to the effect of bracing configurations. CFSS members in Specimen F3 had a large amount of connections to the braces, due to the X-brace configuration instead of the single diagonal, leading a more distributed load pattern on the studs.
5. Although the web crippling capacity of the studs per AISI (1996) was satisfactory for the design loads, upon strain hardening and out-of-plane buckling deformations of the braces, some studs suffered web crippling and local flange bending. Increasing the design load for the studs to account for those effects, or stiffening the flanges and webs of the studs at the connections to the braces, would have improved the performance of the specimens.
6. It is also noted that the pushover analysis envelopes for concentrically braced frames predicted by FEMA 356 (2000) and FEMA 368 (2001) do not represent well the behavior of braced frames, and therefore may need to be improved.

Acknowledgments

This research was supported in part by the Earthquake Engineering Research Centers Program of the National Science Foundation (NSF) under Award Number EEC-9701471 to the Multidisciplinary Center for Earthquake Engineering Research (MCEER). The first writer thanks the Istanbul Technical University (ITU) President Office and ITU Faculty of Architecture for their partial support during his stay in Buffalo, under Grant to Support Long Term Research Activities Abroad for Young Researchers. However, any opinions, findings, conclusions, and recommendations presented in this paper are those of the writers and do not necessarily reflect the views of the sponsors.

References

American Institute of Steel Construction (AISC). (1999). *Load and resistance factor design (LRFD) specification for structural steel buildings*, Chicago.

American Institute of Steel Construction (AISC). (2002). *Seismic provisions for structural steel buildings*, Chicago.

American Iron and Steel Institute (AISI). (1996). *Cold-formed steel design manual*, Washington, D.C.

Applied Technology Council. (1992). "Guidelines for cyclic seismic testing of components of steel structures." *ATC-24*, Calif.

Archambault, M.-H., Tremblay, R., and Filiatrault, A. (1995). "Étude du comportement séismique des contreventements ductiles en X avec profilés tubulaires en acier." *Rapport No. EPM/GCS-1995-09*, Département de Génie Civil, Section Structures, École Polytechnique de Montréal, Québec, Canada.

American Society for Testing and Materials (ASTM). (2002). "Standard test methods and definitions for mechanical testing of steel products." *A 370-97a*, Philadelphia.

Berman, J. W., and Bruneau, M. (2003). "Experimental investigation of light-gauge steel plate shear walls for the seismic retrofit of buildings." *Technical Rep. MCEER-03-0001*, Multidisciplinary Center for Earthquake Engineering Research, Buffalo, N.Y.

Black, C., Makris, N., and Aiken, I. (2002). "Component testing, stability analysis and characterization of buckling-restrained unbonded braces." *PEER Rep. 2002/08*, Pacific Earthquake Engineering Research Center, University of California, Berkeley.

Black, R. G., Wenger, W. A. B., and Popov, E. P. (1980). "Inelastic buckling of steel struts under cyclic load reversals." *Rep. No. UCB/EERC-80/40*, Berkeley, Calif.

Bruneau, M., Whittaker, A. S., and Uang, C. M. (1998). *Ductile design of steel structures*, McGraw-Hill, New York.

Celik, O. C., Berman, J. W., and Bruneau, M. (2004). "Cyclic testing of braces laterally restrained by steel studs to enhance performance during earthquakes." *Technical Rep. MCEER-04-0003*, Multidisciplinary Center for Earthquake Engineering Research, Buffalo, N.Y.

Clark, P. W., Kasai, K., Aiken, I. D., and Kimura, I. (2000). "Evaluation of design methodologies for structures incorporating steel unbonded

braces for energy dissipation." *Proc., 12th World Conf. on Earthquake Engineering, Paper No. 2240*, New Zealand.
Computers and Structures, Inc. (CSI). (1998). *SAP2000 Integrated finite element analysis and design of structures—Detailed tutorial including pushover analysis*, Berkeley, Calif.
Dafalias, Y. F., and Popov, E. P. (1976). "Plastic internal variables formalism of cyclic plasticity." *J. Appl. Mech.*, 43, 645–651.
Dietrich Industries, Inc. (2001). "Curtain wall/light gage structural framing products." *ICBO No. 4784P, LA RR No. 25132*.
Federal Emergency Management Agency. (2000). "Prestandard and commentary for the seismic rehabilitation of buildings." *FEMA 356*, Washington, D.C.
Federal Emergency Management Agency. (2001). "NEHRP recommended provisions for seismic regulations for new buildings and other structures: Part 1-Provisions." *FEMA 368*, Washington, D.C.
Filiatrault, A., and Tremblay, R. (1998). "Design of tension-only concentrically braced steel frames for seismic induced impact loading." *Eng. Struct.*, 20(12), 1087–1096.
Ikeda, K., and Mahin, S. A. (1984). "A refined physical theory model for predicting the seismic behavior of braced steel frames." *Rep. No. UCB/EERC-84/12*, Berkeley, Calif.
Iwata, M., Kato, T., and Wada, A. (2000). "Buckling-restrained braces as hysteretic dampers." *Proc., 3rd Int. Conf. on Behavior of Steel Structures in Seismic Areas (STESSA 2000)*, Montreal, Canada, 33–38.
Ko, E., et al. (2002). "Application of the unbonded brace in medical facilities." *Seventh U.S. National Conf. on Earthquake Engineering (7NCEE)*, Paper No.16, Boston (CD-ROM).
Lee, K., and Bruneau, M. (2002). "Review of energy dissipation of compression members in concentrically braced frames." *Technical Rep. MCEER-02-0005*, Buffalo, N.Y.
Lee, S., and Goel, S. C. (1987). "Seismic behavior of hollow and concrete-filled square tubular bracing members." *Rep. No. UMEE 87-11*, Department of Civil Engineering, University of Michigan, Ann Arbor, Mich.
Remennikov, A. M., and Walpole, W. R. (1997). "Analytical prediction of seismic behavior for concentrically-braced steel systems." *Earthquake Eng. Struct. Dyn.*, 26, 859–874.
Salmon, C. G., and Johnson, J. E. (1996). *Steel structures—Design and behavior*, 4th Ed., Prentice-Hall, Englewood Cliffs, N.J.
Tremblay, R. (2002). "Inelastic seismic response of steel bracing members." *J. Constr. Steel Res.*, 58, 665–701.
Winter, G. (1960). "Lateral bracing of columns and beams." *Trans. Am. Soc. Civ. Eng.*, 125, 807–845.
Yang, T. Y., and Whittaker, A. (2002). "MCEER demonstration hospitals—Mathematical models and preliminary results." *Technical Rep.*, Multidisciplinary Center for Earthquake Engineering Research, University at Buffalo, Buffalo, N.Y.
Yura, J. A. (1993). "Fundamentals of beam bracing." *Is Your Structure Suitably Braced?, Structural Stability Research Council, 1993 Conf.*, Milwaukee, Wis.
Yura, J. A. (1994). "Winter's bracing approach revisited." *Proc., 50th Anniversary Conf., Structural Stability Research Council*, Lehigh University, 375–382.
Zayas, V. A., Mahin, S. A., and Popov, E. P. (1980). "Cyclic inelastic behavior of steel offshore structures." *Rep. No. UCB/EERC-80/27*, Berkeley, Calif.